Hard X-Ray Spectrometer (HXS) Conceptual Design

April 7, 2000

Principal Investigator: Dr. John F. Seely
Head, UV and X-Ray Spectroscopy Section
Space Science Division, Code 7674
Naval Research Laboratory
Washington DC 20375-5352
Tel: 202-767-3529 Fax: 202-404-7997
E-mail: john.seely@nrl.navy.mil

Co-Investigators: Drs. Richard Deslattes & Lawrence T. Hudson
National Institute of Standards and Technology
Gaithersburg MD 20899

Contents

1. Abstract
2. Optical Conceptual Design
3. Electronic Conceptual Design
4. Expected X-Ray Spectra
5. Sensitivity Estimation
6. Characterization of the Plate Function at NIST
7. Operational Characterization using the NRL Pulsed X-Ray Source
8. References

1. Abstract

A Hard X-Ray Spectrometer (HXS) will be designed, built, and fielded in a TIM at the OMEGA laser facility for the purpose of recording the hot-electron Bremsstrahlung energy distribution in the x-ray energy range 12 to 60 keV region. The spectrometer is an adaptation of a compact and robust instrument that was originally developed at NIST for the energy calibration of medical radiography x-ray sources. The spectrometer is composed of a cylindrically bent crystal, slit, scatter shielding, and a detector plane that is compatible with a CCD camera or a streak camera. A CCD x-ray detector will be provided with the instrument. The CCD is detachable so that the spectrometer can be mounted on an LLE streak camera for the purpose of recording time-resolved spectra. Based on preliminary sensitivity tests of a prototype spectrometer and the expected hard x-ray flux from OMEGA targets, well-exposed spectra can be recorded on the CCD on a single laser shot. In addition, it has been determined that spectra can be acquired on a single shot from a small, pulsed laboratory x-ray source. This source will be used for the operational testing of the spectrometer and the CCD detector. A characterization of the spectrometer's plate function (energy scale) will be performed at NIST.

2. Optical Conceptual Design

The optical design is a modification of the x-ray spectrometer that was previously developed at NIST (see Fig. 1).[1,2,3] A sketch of the present optical design for the LLE application is shown in Fig. 2. The cylindrically bent crystal is positioned at a distance of 500 mm from the OMEGA target. The x-rays are incident on the entrance apertures, diffracted by the crystal, converge through a slit aperture, and are incident on the detector plane at a distance of 118 mm from the entrance apertures. The energy coverage is 12-60 keV. Shown in Fig. 2 is a detachable CCD assembly. When detached, the spectrometer box can be mounted on an LLE streak camera so that the spectral image falls on the photocathode. The overall size of the spectrometer box is 118 mm long and 107 mm wide.

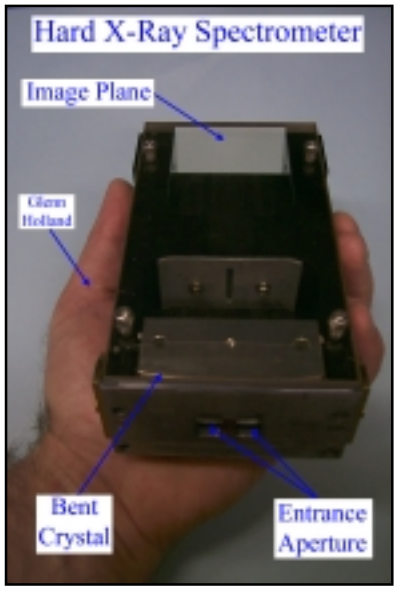

Fig. 1. Photograph of a spectrometer designed for the energy calibration of medical radiography x-ray sources.

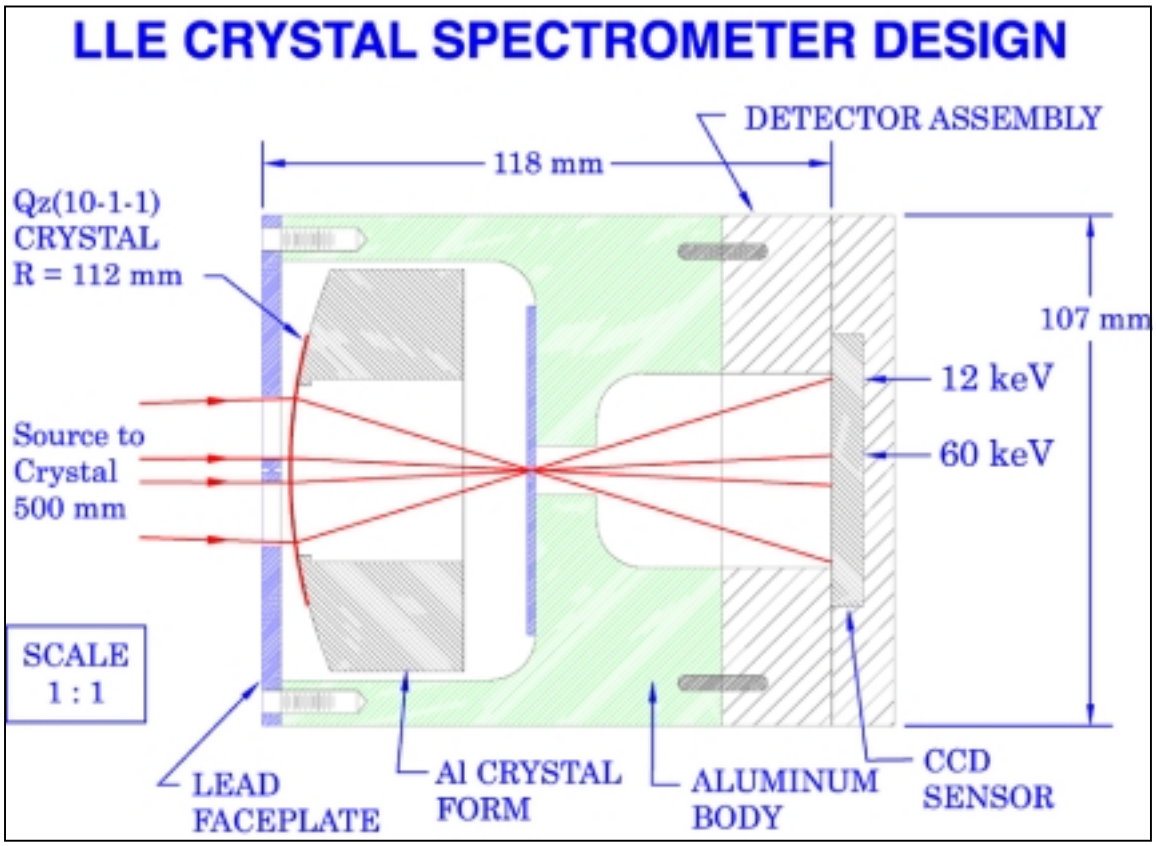

Fig. 2. Optical design of the LLE spectrometer.

Based on the expected x-ray spectral distribution, the crystal thickness, bending radius, and diffraction planes have been be optimized for the OMEGA application. The crystal is quartz using the (1,0,-1,-1) reflection, and the bending radius is 112 mm.

The integration of the spectrometer to the TIM cart will be carried out at NRL using a existing TIM boat and a target setup fixture that simulates the OMEGA geometry. The single-shot performance of the spectrometer will be characterized using a pulsed x-ray source. Aside from its x-ray diffraction characteristics, quartz's transparency to visible light should simplify alignment verification in the laboratory. A standard LLE pointer will be implemented for alignment to the OMEGA target.

The lead faceplate and the lead shielding around the slit aperture prevent x-rays from directly reaching the detector. A light-tight x-ray filter covers the slit aperture. A Be debris filter is positioned in the nosecone of the instrument.

The crystal form, spectrometer box, and CCD mounting hardware will be manufactured at NIST. The CCD detector, electronics, and data acquisition system will be provided by NRL

3. Electronic Conceptual Design

The HXS electronic system will consist of three basic parts: Diagnostic Control Processor (DCP), Diagnostic Interface Unit (DIU), and the diagnostic itself. The DCP will interface to the OMEGA system and will accept, and respond to, OIP messages from the control system, including shot preparation, control, status, and data request messages. A DCP-resident daemon will process these messages via a TCP/IP socket connection. The DCP will also contain a user interface for stand-alone operation. This user interface will communicate with the DCP server via a TCP/IP socket with the same command/control interface as the OMEGA control system (OIP). This method will maximize code and functionality reuse.

The DCP will connect to the HXS via the DIU. The DIU will convert the copper RS232 interface to a single-fiber full-duplex communication link. A positive acknowledgement, error-checked, packet-based protocol will be used over this link to ensure data integrity and command reception. A second fiber will be used to convey shot timing information (most notably the T-10 pulse and possibly the shot termination). The DIU will accept an electrical signal from the OMEGA system (via a BNC) indicating the T-10 timing pulse. This information will be converted to the required fiber-based format.

The DCP will be able to request a Built-In-Test from the HXS electronics. It will use the results of the BIT along with its own readiness tests to generate the required *READY* messages for the OMEGA control system. The DCP will also handle all anomaly conditions (abort, etc) and archive the state-of-health (SOH) information returned from the diagnostic (battery information, etc). This information may be tracked or discarded depending upon the situation. (As an aside, an electronic dosimeter could easily be integrated into the device and the dose rates tracked long-term as well as across individual shots).

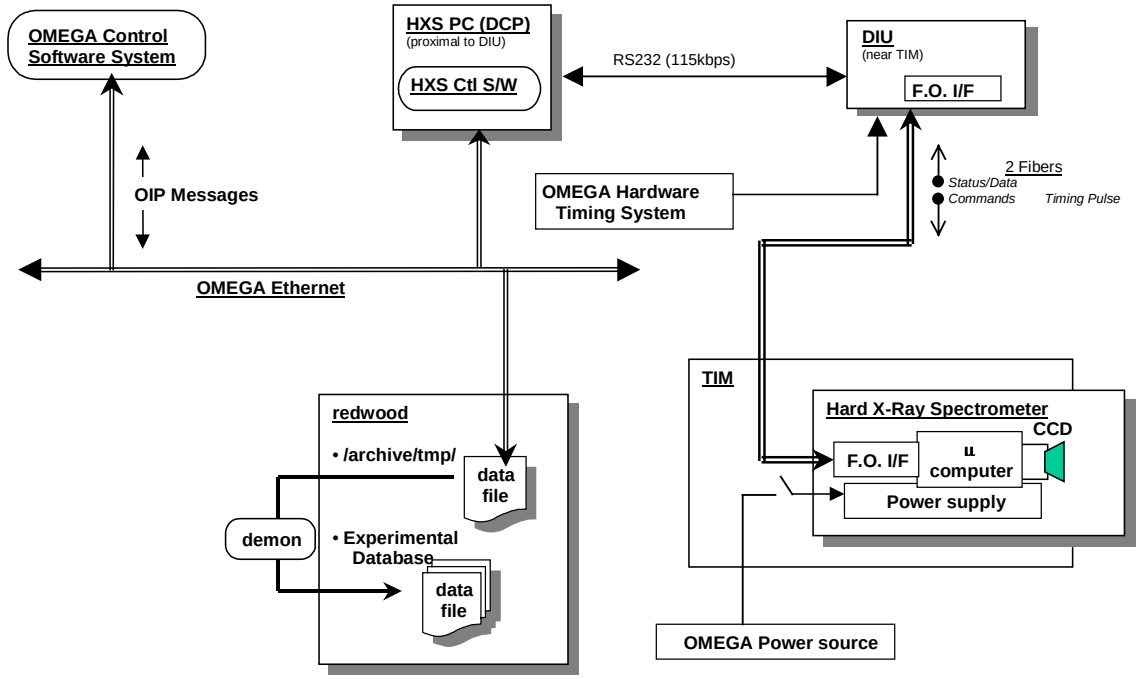

The HXS itself will have several components. The power supply will generally provide battery power to the unit. This will enable the HXS to provide a minimum of interference to the remainder of the system (and be minimally susceptible to the external environment); the only interface will be an optical one. Optionally the HXS will be able to switch to externally supplied power, which may be required for battery recharge, operation during battery failure, or extremely long-duration testing (depending upon the power consumption of the device: see the discussion below).

There will be a low-power micro-controller based control unit. This unit will monitor the health of the overall experiment, including various temperatures, voltages, and currents. This SOH information will be regularly reported to the DCP for archive/analysis. The unit will also control the power supply, interface to the outside world via the fiber-optic link, and handle the precision shot-timing pulses to the CCD. The power filtering and fiber-optic conversion circuitry will also be integrated in this unit.

The HXS will also contain the CCD and its associated control electronics. The final component of the instrument is the interface between the CCD control electronics and the HXS control unit. This component has several issues that are discussed below in more detail.

This operations concept effectively divorces the actual diagnostic from the system in which it is being used. The DCP will provide the proper interface between the diagnostic and the overall system. The diagnostic can be designed to be as simple as possible (and therefore as low-power as possible, enabling continuous battery operations). The design keeps the basic control environment the same for on-line operations as the test phase (as far as the DCP and instrument are concerned). In addition, the diagnostic EGSE tools will be instantly available, without breaking configuration, in the unlikely event on-site trouble-shooting is necessary.

The CCD control electronics have two interfaces: PCI and USB. Their operational details are presently being investigated. For example, there are several different modes of operation that might be possible: the control electronics read the CCD data and store it locally for later transmission; the USB simply begins to send data when the integration phase is complete; the PCI begins to DMA the data at the end of the integration phase; the main USB/PCI controller must orchestrate all data transfer from the CCD at the proper time; other, more bizarre, data transfer mechanisms. Perhaps (this is probably a big perhaps) the PCI/USB control electronics can be dispensed with altogether and a custom interface directly to the CCD used in its place (advantages : lower-power, simpler interface to micro-controller, lower long-run cost; disadvantages: possibly longer development, more complex electronics). Each of these scenarios pose different engineering problems, with (in many cases) vastly different solutions.

It is obvious that some experimentation is in order. The first development path is to use a COTS PC/104+ single board computer for the interface to the control electronics. There is one to be had (pentium-based) which has 2USB ports, PCI, serial, and disk-on-a-chip. We will experiment with both the PCI and USB interfaces, including characterizing the CCD (both in single- and multi-sensor configurations). The software will be easy to develop, and probably partly reusable. The SBC would interface to the HXS control unit via one of the serial ports (or maybe the ISA bus). The interface can be made generic enough that the control unit will require little (if any) software modification to run with the PC/104+ SBC versus the custom board (second path). If necessary this configuration can be fielded to LLE (the down side is the COTS board will consume much more power than the custom interface, at least at first

analysis). The SBC could be left powered off until it is needed (power control provided by the control unit) to drastically reduce overall power consumption.

The second development path is to implement a custom board based on some of the experimentation (with the COTS PC/104, with a PC, and generic experimentation with the devices). It may turn out that it becomes obvious immediately that this option is not needed. A USB interface board can be developed with a three-chip chipset and a micro-controller (plus associated electronics). This chipset is the only embedded root-hub on the market. Supposedly, several other single-chip integrated root-hub/micro-controller are currently under development, but are several months away (actually an FPGA design is available, but an unrestricted license is costly, although they said they could go as low as approximately $20,000 for us if we would sign an agreement to only use the design for this instrument and would forego technical support). The basic idea would be to perform a proof-of-concept with the current technology with the idea of replacing the majority of the components with one of the new devices (reducing complexity and especially power).

4. Expected X-Ray Spectra

The instrument produces two spectral representations that are mirror images of one another. The instrumental zero wavelength position lies at the bisector of any pair of corresponding spectral features. This permits the energy axis to be easily calibrated using a few x-ray lines. Although the wavelength dispersion is approximately constant, a more accurate representation of the "plate function" is given by:

$$E^2 = a*x^{-2} + b$$

where a and b are constants, x is the distance from the center of the two mirror spectra, and E is the energy of the spectral bin at x. This function is plotted in Fig. 3(a) for the instrument design. The corresponding spectral resolving power, assuming a detector spatial resolution of 50 μm, is shown in Fig. 3(b).

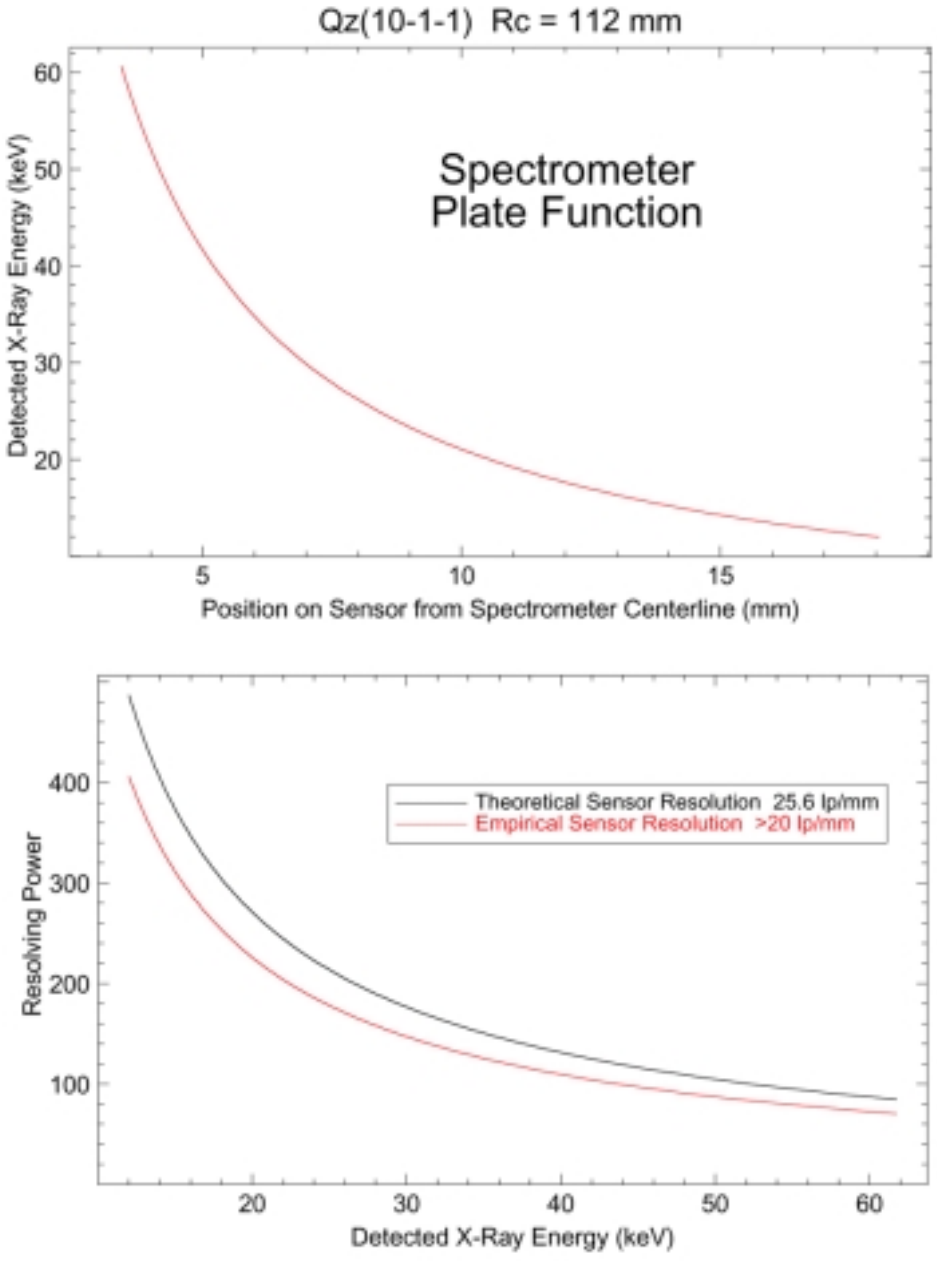

Fig. 3 Part (a) shows the plate function for the 12-60 keV design. Part (b) indicates the resolving power that will be available using a 50 micrometer resolution imager.

Spectra obtained from a thick molybdenum target using a previously developed NIST spectrometer and a CCD are shown in Fig. 4 for several accelerating potentials. The lower energy regions were excluded from these pictures by geometrical restrictions, the use of relatively thick crystals, and a detector/phosphor combination optimized for the 20-40 keV region.

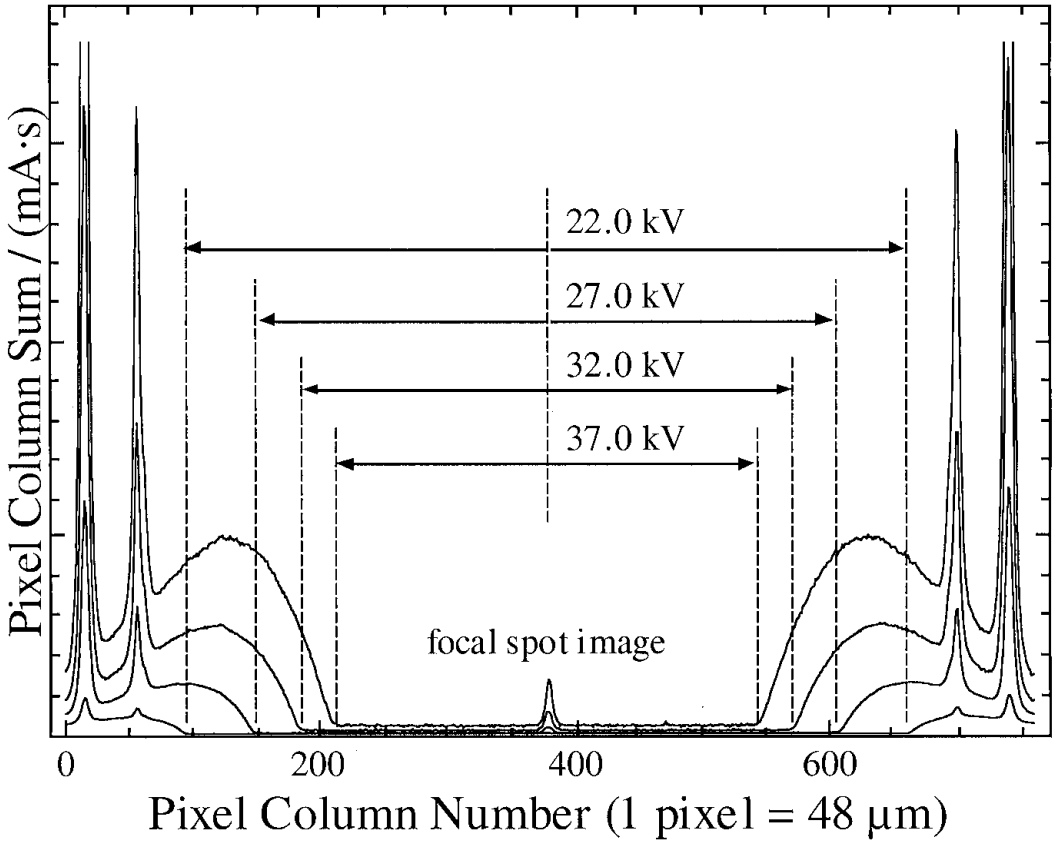

Fig. 4. Thick target Mo spectra (1 mm Al filtration) obtained by summing the CCD pixel columns after a dark image subtraction. The crystal was bent to 15 cm radius of curvature. Exposures were below 60 mA-s.

5. Sensitivity Estimation

In previous work on a similar spectrometer design, we carried out a sequence of measurements in which the imaging detector was replaced by a scanning NaI x-ray scintillation counter behind a well-defined aperture. The slit-limited detector was mounted on a mechanical stage that could be moved through the entire region of interest. In the range of energies considered, the NaI detector used had more than 75% quantum efficiency. The aperture was approximately 50 μm wide, 1.5 cm high, and at a distance of 21.1 cm from the source, thereby intercepting a solid angle fraction of 1.3×10^{-6}. Spectra so acquired give the number of x-rays in a given bandwidth and solid angle arriving at the detector plane. When coupled with the source brightness, calculated below, an estimate of spectrometer sensitivity follows.

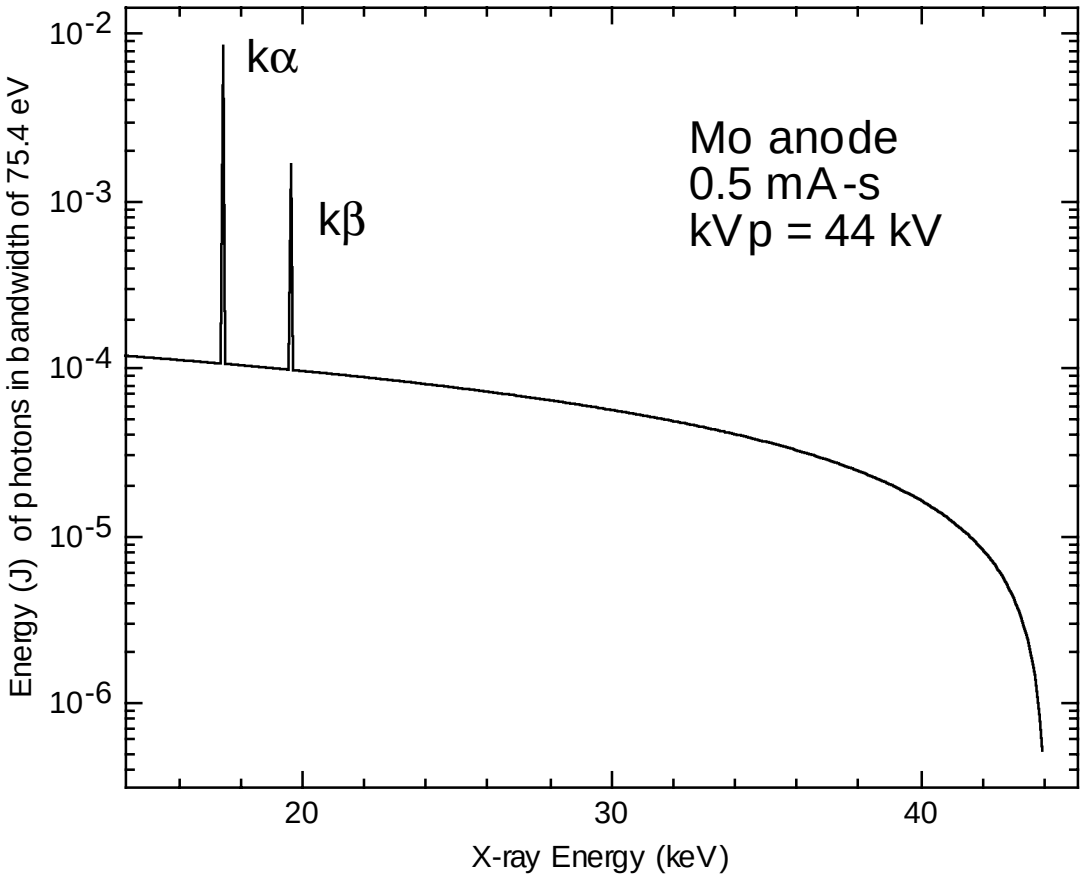

Fig. 5. Calculated source energy spectrum.

The source of x-rays was a conventional Mo target diffraction tube with a nominal focal spot 1.3 mm wide and 12.5 mm long. It was viewed "end-on" with a takeoff angle of 6° yielding a more or less square source. Thick target bremsstrahlung from such a source is well described by the Kramers' formulation as regards to both overall spectral shape and the efficiency with which electrical power input to the x-ray source is converted into total x-ray power. (The particular tube used was an old one whose output is likely to be less than these estimates suggest.) The spectral output calculated for the conditions under which data were acquired is shown in Fig. 5 as computed by commercial software employing the Kramers' formulae. It is presented as the total energy of the x-rays, in joules, emitted at the source into 4π per 75.4 eV energy interval. This energy bandwidth was chosen to correspond to the spectral acceptance of the 50 μm slit at the intermediate x-ray energy of 21.5 keV. The theoretical x-ray 'power' can then be read off Fig. 5 at 21.5 keV to be 9.175×10^{-5} J (per 1 sec). Dividing 21.5 keV into this gives 2.67×10^{10} x-rays at this energy/sec/75.4 eV bandwith/4π. The NaI detector registered 1224 x-rays per/sec/75.4 eV bandwidth at 21.5 keV. Hence, spectrometer efficiency times solid angle is estimated to be 5×10^{-8} at intermediate energies.

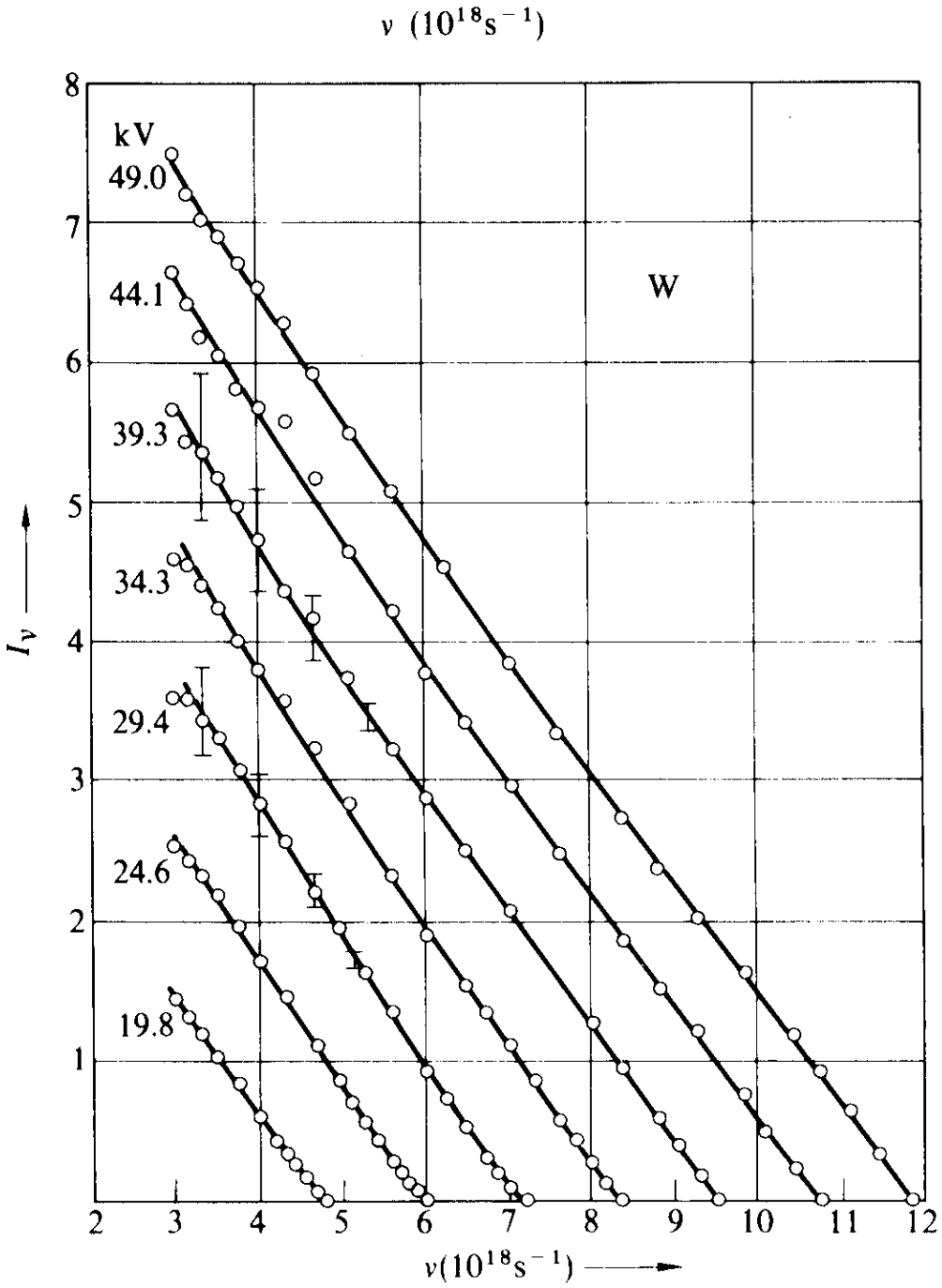

Fig. 6. Thick target bremsstrahlung measured by Kuhlenkampff, H. and Schmidt, L (1943) Ann. Der Phys., 43, p. 494.

As a check of the output spectrum of the commercial software, we note that with the anode and energy at which these data were acquired, the thermodynamic efficiency is about $1.3x10^{-6} \bullet Z \bullet V(kV) = 0.0024$. With the x-ray tube set at 44 keV and 0.5 mA, the 22 W of electrical energy then results in 0.0528 W of x-rays emitted into 4π. Kuhlenkampff and Schmidt have shown that when the intensity of bremssrahlung radiation is plotted against energy, a quite linear relationship is found with I(kVp) = 0 (see Fig. 6). We can assign the area of this "right triangle" to the total x-ray power emitted, or 0.0528 W, thereby establishing the y-intercept and slope for our model intensity distribution. Finally, the power in a vertical slice of this intensity distribution with an energy bandwidth comparable to that captured by the slit ($5.79x10^{11}$ keV/s into the 75.4 eV bandwidth) can be divided into the countrate obtained by the NaI detector times photon energy. This again gives a value of spectrometer efficiency times solid angle of about $5x10^{-8}$ at 21.5 keV.

Christian Stoeckel, of LLE, has estimated the spectrum from the OMEGA laser to be a function of the form exp(-E/kT) with kT in the range between 50 to 100 keV. He further estimated that the total energy radiated into 4π was between 0.1 to 1 J. This suggests the spectrum shown in Fig. 7(a), which is intensity integrated over the time of a single laser shot or total number of x-ray photons emitted as a function of energy for 0.1 J of emitted x-ray power, *viz*, $1.248x10^{13} \bullet \exp(-E/50\ \text{keV})$. This is converted into an energy spectrum in Fig. 7(b) and then compared with the energy spectrum from the Mo tube under the conditions of 44 keV (Fig. 7(c)). The Mo spectrum is identical to the energy spectrum of Fig. 5 except that it has been scaled upward to represent the total energy spectrum emitted in 4.6 mA•s from a 44 kV Mo x-ray tube. This is the exposure which gave an acceptable spectrum on a dental CCD detector system at a source to spectrometer distance of 21 cm. Finally, in Fig. 8 we present a comparison of these same two energy spectra normalized to solid angle subtended. The presently proposed spectrometer design is for a source to spectrometer distance of 50 cm. Hence, the upper curve of Fig. 8 has been scaled down from Fig. 7(c) by the ratio of the squares of these two distances. This result estimates that the OMEGA laser as seen by the spectrometer at 50 cm is a factor of two brighter at 10 keV relative to a Mo x-ray tube (44 kV) at 21 cm. At higher energies, the OMEGA laser compares even more favorably. (This relative comparison of sources is not to be confused with the spectrometer sensitivity function as a function of energy.)

One should note this estimate contains uncertainties, including: the energy dependent efficiency of the NaI detector, the lifetime-dependent intensity of the Mo tube, the brightness and spectral distribution of OMEGA, and differences in the spectrometer designed for OMEGA which include radius of curvature, and the use of a detector with different system efficiency than the one used above to obtain an "acceptable" image.

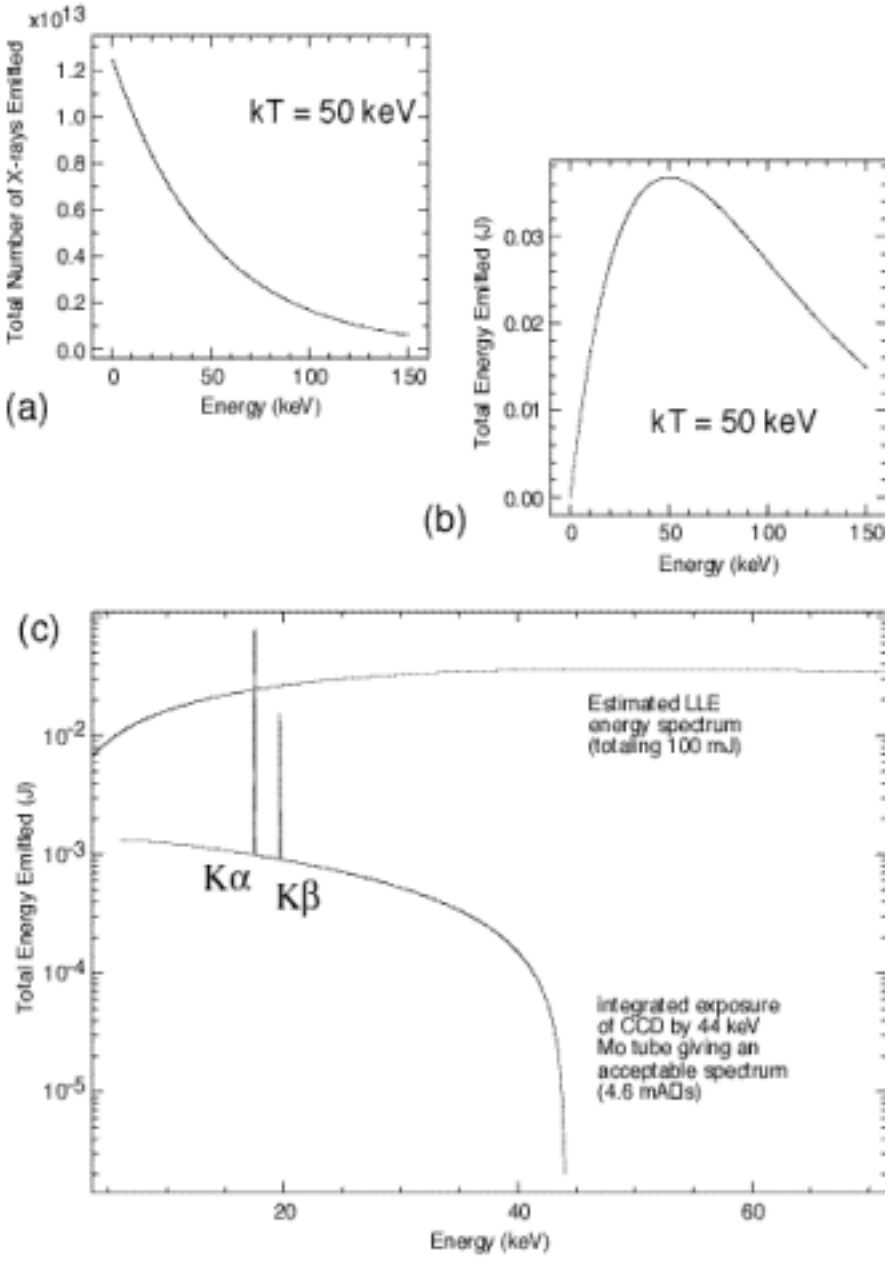

Fig. 7. (a) Modeled intensity spectrum of the OMEGA laser with kT = 50 keV and area under the curve equal to 0.1 J. (b) Intensity spectrum converted to an energy spectrum. (c) Comparison of source spectra from OMEGA and an integrated exposure from a Mo tube.

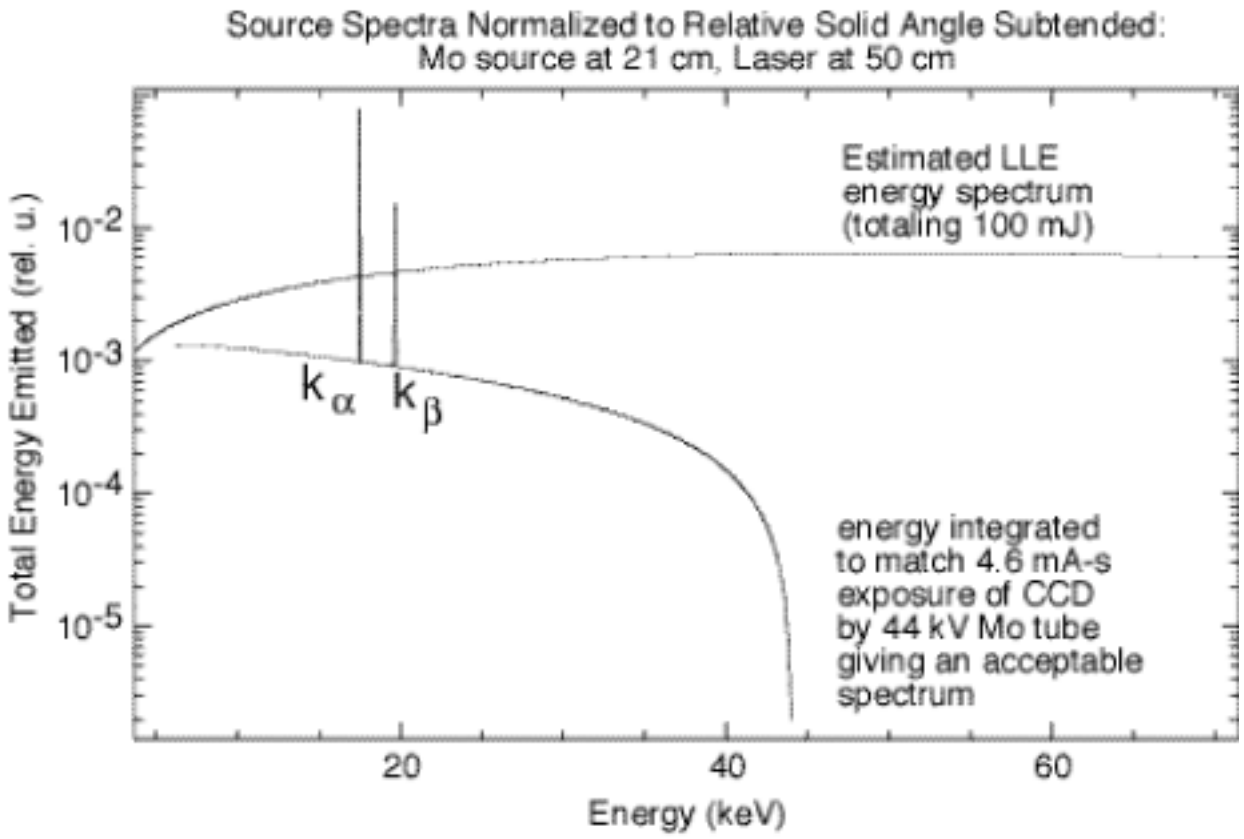

Fig. 8. This is a perturbation of Fig. 7(c). The presently proposed spectrometer design is for a source to spectrometer distance of 50 cm. Hence, the upper curve has been scaled down by the ratio of the squares of these two distances for comparison with a Mo exposure giving an 'acceptable' spectrum.

6. Characterization of the Plate Function at NIST

The characterization process is intended to proceed in an iterative fashion. First, characteristic line spectra will be obtained from three solid-target sources, such as Mo, Rh and Ag with characteristic lines in the region of interest. These will be used to verify the expected resolution and provide well-defined energy calibration points on the image plane, establishing the plate function for the spectrometer at 50 cm from the source. Next, bremsstrahlung spectra from targets having no characteristic lines in the region of interest will be used to provide source-based radiometric calibration, based on Kramers' description of thick target bremsstrahlung, as was described above.

Thick-target bremsstrahlung can also be used to extend the energy scale calibration by mapping the region near the high energy cutoff of this continuous spectrum. At this spectroscopic limit, the radiated energy $E = h\nu = eV$ is numerically equal to the voltage difference applied across the x-ray tube. The spectrometer design is well suited to obtaining

good data near this limit and it is being developed commercially as a non-invasive high voltage measuring system. Conversely, by operating the source at a series of well-defined accelerating potentials, we can conveniently extend the region covered by available characteristic sources to the present upper limit of 60 keV. This same result could also be obtained using characteristic lines of heavier elements such as Ta (60 keV) or W (63 keV). However, efficient production of these lines requires accelerating voltages near or above 100 kV that are not currently available in our local laboratory.

7. Operational Characterization using the NRL Pulsed X-Ray Source

The operation of the spectrometer and CCD will be characterized using a pulsed laboratory x-ray source described below. In preparation for this work, single-shot spectra have been recorded by the NIST spectrometer on Polaroid film, and high resolution multi-shot spectra were recorded on DEF film (see Fig. 9). The anode was Mo, and the peak voltage was 150 kV. The Mo Kα1 and Kα2 lines at 17.48 and 17.37 keV were resolved in the DEF spectra, indicating a resolving power of approximately 300. A single-shot spectral image recorded on Polaroid film and using a W anode with 150 kV voltage is shown in Fig. 10. The image is of the W continuum in the 12-20 keV x-ray energy range; the W K lines are beyond the coverage of this particular spectrometer.

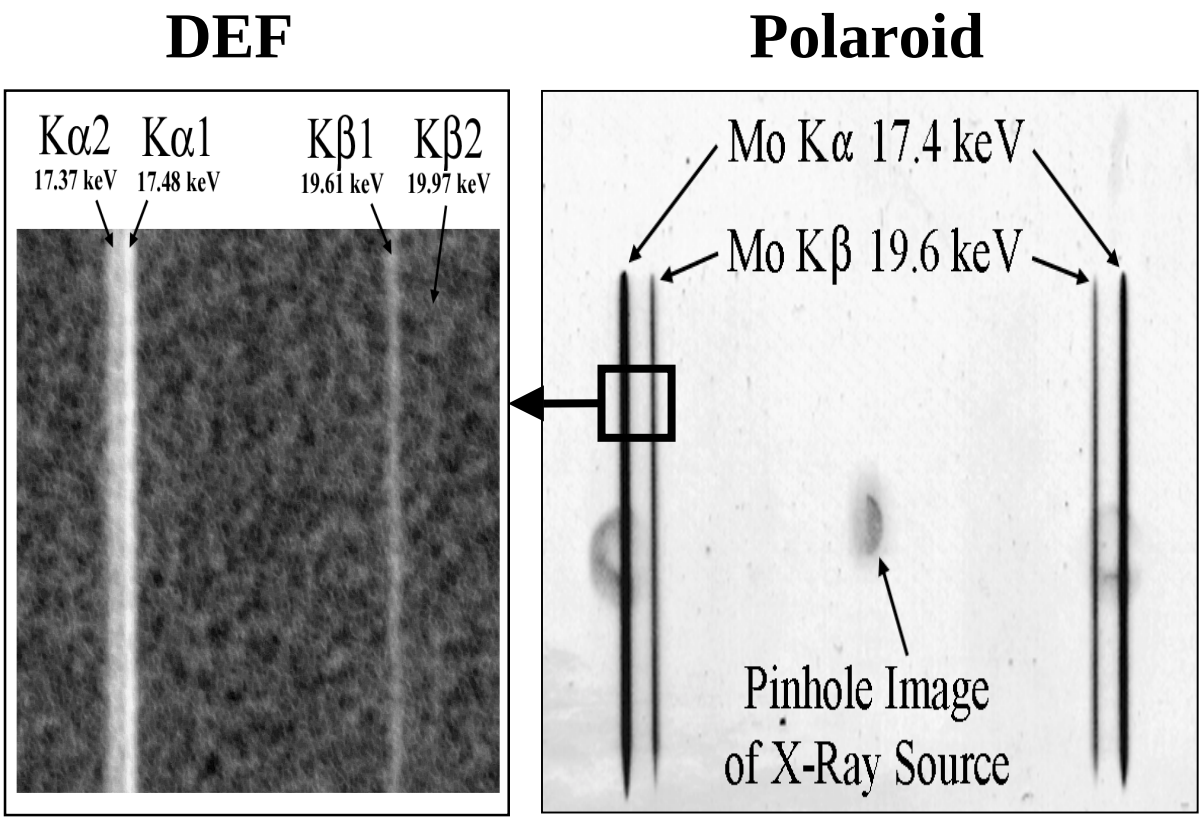

Fig. 9. Spectral images recorded using a pulsed laboratory x-ray source with a Mo anode.

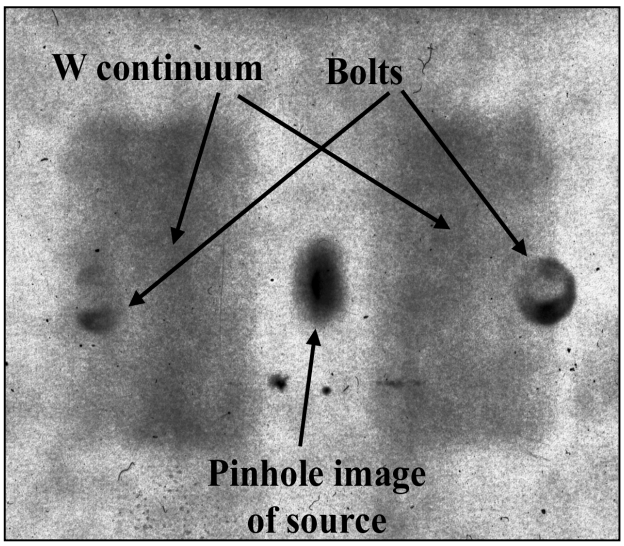

Fig. 10. Spectral image recorded on Polaroid film of the continuum from the pulsed x-ray source with a W anode.

The spectral images shown in Figs. 9 and 10 were recorded by the pulsed laboratory x-ray source shown in Fig. 11. The source consists of a Marx generator with 15 energy storage capacitors, a cold field emission x-ray tube, control electronics, and a rechargeable battery. The Marx generator can be charged to approximately 200 kV and normally stores 5 J of electrical energy. As part of a NASA project, a unit is being developed that has 30 capacitors and 10 J stored energy. These units will be utilized for the characterization and optimization of the x-ray spectrometer and the detector electronics.

The x-ray source has been extensively tested and evaluated using voltage and current probes and a 1 GHz digitizing oscilloscope with 5 GHz sampling.[4] The data from 13 consecutive shots are shown in Fig. 12. The variation in the peak voltage was 2%, and the variation in the x-ray flux measured by a fast silicon diode was 8%.

A detailed model for the x-ray source was formulated. The equivalent circuits are shown in Fig. 13. The set of 16 equations was solved using a fourth-order Runge-Kutta algorithm, and the calculated results are shown in Fig. 14. The calculated results include the currents in the trigger circuit and in each storage capacitor and the diode, the voltages in each storage capacitor and the diode, the diode power and impedance, and the diode perveance and delivered charge.

The calculated and measured data indicate an initial electron acceleration phase characterized by high tube perveance with a rapid increase in the tube current and voltage. This is followed by an arc phase in which the current continues to increase while the voltage and impedance across the tube rapidly collapse in the ensuing vacuum arc. The x-ray energy is relatively high early in the pulse (when the electron acceleration voltage is high) and decreases later in the pulse.

Using a W anode, the x-ray source produces an exposure of 34 mR measured at a distance of 30 cm. The measured exposure is in good agreement with the calculated x-ray exposure. The energy in the characteristic W K x-ray lines is 0.8 mJ, and the energy in the

continuum is 16 mJ. The efficiency of conversion from electrical energy to x-ray energy is 0.34%.

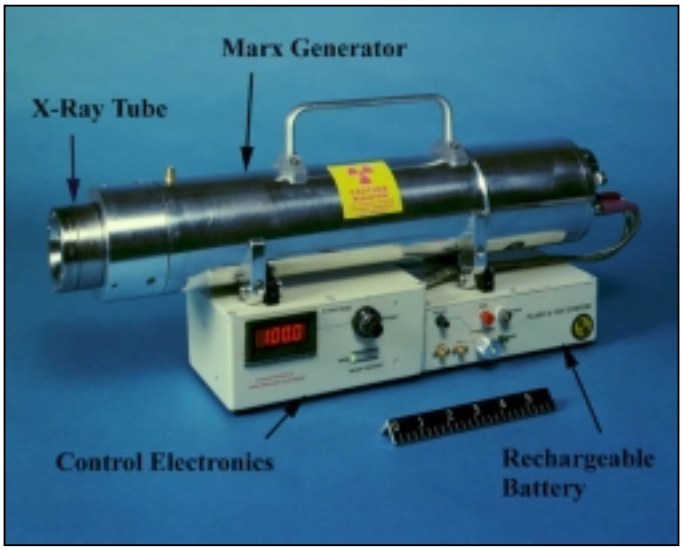

Fig. 11. The pulsed x-ray source showing the Marx generator, x-ray tube, control electronics, and rechargeable battery.

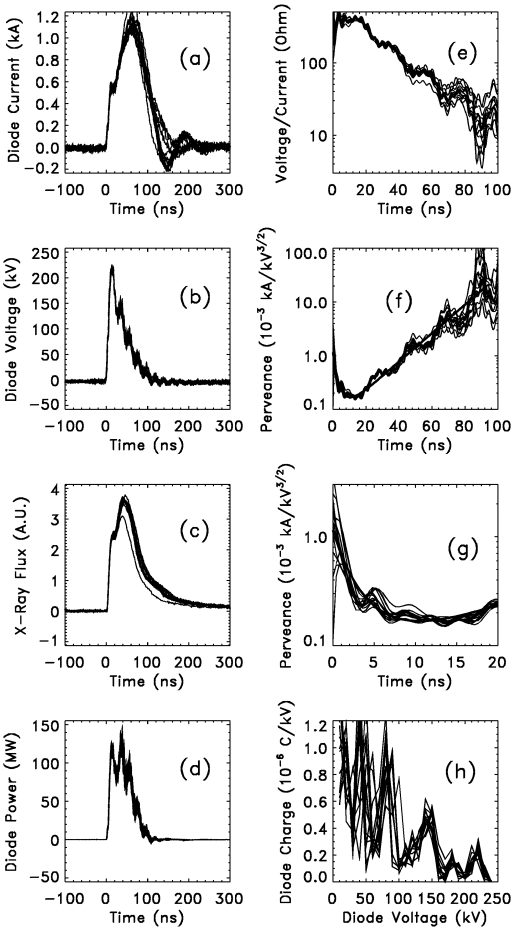

Fig. 12. The measured data for 13 consecutive shots of the pulsed x-ray source. (a) Diode current, (b) diode voltage, (c) x-ray flux, (d) diode power derived from the current and voltage, (e) impedance, (f) and (g) perveance derived from the current and voltage, and (h) charge delivered to the diode.

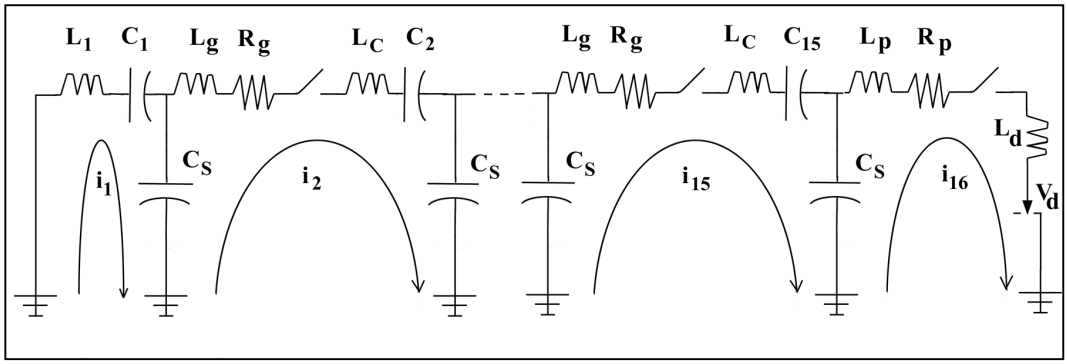

Fig.13. Equivalents circuits for the pulsed x-ray source: Trigger (state 1), Marx generator (stages 2-15), and x-ray tube (stage 16).

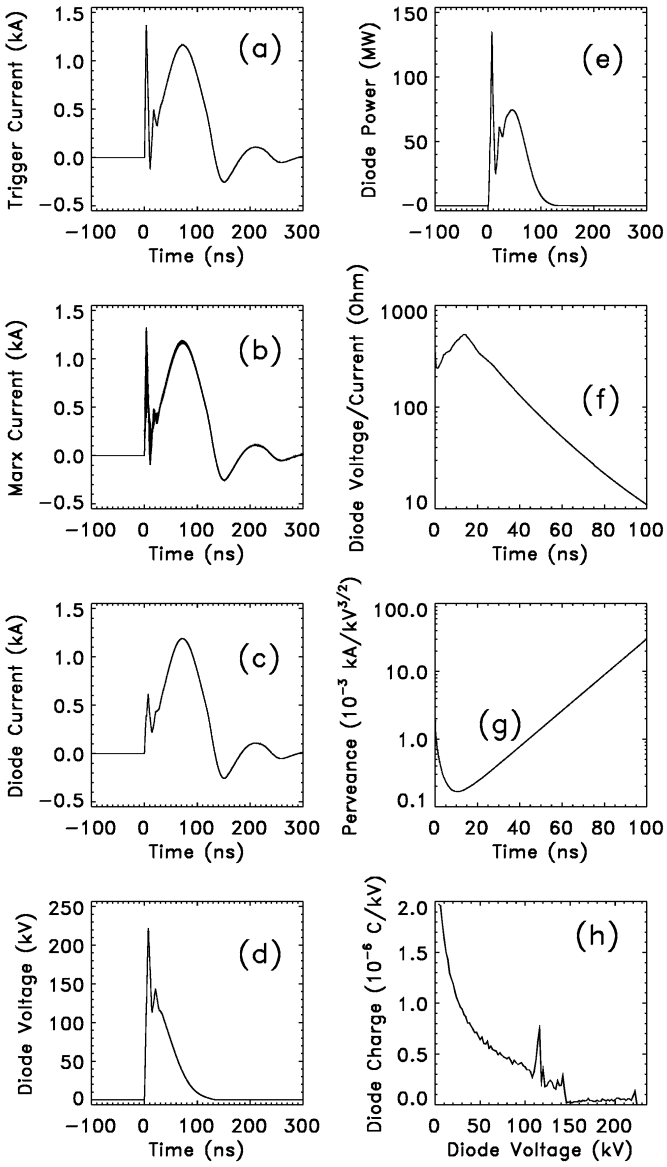

Fig. 14. The calculated results. (a) Trigger current, (b) Marx current, (c) diode current, (d) diode voltage, (e) diode power, (f) diode impedance, (g) perveance, and (h) charge.

8. References

1. R. D. Deslattes, J. C. Levin, M. D. Walker, and A. Henins, "Noninvasive High-Voltage Measurement in Mammography by Crystal Diffraction Spectrometry," Med. Phys. **21**, 123 (1994).
2. L. T. Hudson, R. D. Deslattes, A. Henins, C. T. Chandler, E. G. Kessler, and J. E. Schweppe, "A Curved Crystal Spectrometer for Energy Calibration and Spectral Characterization of Mammographic X-Ray Sources," Med. Phys. **23**, 1659 (1996).
3. C. T. Chantler, R. D. Deslattes, A. Henins, and L. T. Hudson, "Flat and Curved Crystal Spectrography for Mammographic X-Ray Sources," Br. J. Radiol., **69** 636 (1996).
4. C. N. Boyer, G. E. Holland, and J. F. Seely, "Portable Hard X-Ray Source for Nondestructive Testing and Medical Imaging," Rev. Sci. Instr. **69**, 2524 (1998).